A Sestan et al.

Tungsten carbide as deoxidation agent for plasma-facing tungsten based materials

Tungsten carbide as deoxidation agent for plasma-facing tungsten based materials

Andreja Šestan [1, 2, 3], Janez Zavašnik [1, 3], Marjeta Maček Kržmanc [4], Matej Kocen[2, 5] Petra Jenuš [5], Saša Novak [5], Miran Čeh [1, 2, 5], Gerhard Dehm [3]

[1] Centre for Electron Microscopy and Microanalysis, Jožef Stefan Institute, 1000 Ljubljana, Slovenia

[2] Jožef Stefan International Postgraduate School, 1000 Ljubljana, Slovenia

[3] Max-Planck-Institut für Eisenforschung GmbH, 40237 Düsseldorf, Germany

[4] Advance Materials Department, Jožef Stefan Institute, 1000 Ljubljana, Slovenia

[5] Department for Nanostructured Materials, Jožef Stefan Institute, 1000 Ljubljana, Slovenia

Abstract

Tungsten (W) and its composites are considered primary plasma-facing materials in fusion reactors. All engineering materials, they contain small amounts of impurities, which play an important role in the mechanical properties of the material. In present work, oxygen was identified as a major impurity in our starting tungsten powder. At elevated temperature, the presence of interstitial elements such as oxygen will lead to the formation of oxide-rich tungsten phase at tungsten grain boundaries. In this study, we elucidate the WC nanoparticles capacity to removal oxide impurities from W-body. W composites with 0.05, 0.25 and 0.51 wt. % C in form of WC were sintered via Field-Assisted Sintering Technique (FAST) at 1900 °C for 5 min. The sintered sample were characterized using field-emission scanning electron and transmission electron microscopy. Thermodynamic and kinetic consideration allowed us to determine theoretical optimum amount of WC to prevent the *in-situ* formation of WO_2.

Keywords: tungsten, tungsten carbide, oxide, FAST, FUSION

1. Introduction

Nuclear fusion is one of the most promising clean and safe energy supply for future generation [1]. The extreme conditions in a fusion reactor require the development of suitable materials to achieve the highest possible resistance to heat, particle and neutron loads [2]. Tungsten (W) is a foreseen candidate material for the first wall and the main armour material for the divertor part of the demonstration fusion reactor (DEMO) [3]. Its main disadvantage is relatively poor oxidation resistance at elevated temperature; therefore, sintering is performed in a protective gas atmosphere or in

vacuum conditions [4]. Different powder metallurgy process can be used to produce highly dense W, nevertheless high temperature and protracted sintering time is required because of tungsten's high melting point. *Field-Assisted Sintering Technique* (FAST) was proposed to improve the sintering process of W and to minimise grain-growth during the sintering. FAST processing takes place under vacuum or in inert atmosphere (i.e. nitrogen or argon), while electrical current is applied through the starting powder to generate heat, simultaneously with the application of uni-axial pressure. In FAST we can achieve very high heating rates, leading to an magnitude shorter sintering cycle compare to conventional sintering. It has been reported that high-dense W products are achievable in a relative low sintering temperature when processed by FAST [5, 6]. However, FAST sintering of W has also some drawbacks, such as the direct carbon contamination from the FAST graphite tooling setup [4, 6] and *in-situ* formation of the secondary phase, WO_2 [7, 8].

The impurities could originate from raw powders, collected during various steps during metal processing. The interstitial elements play an important role in the technology of the refractory metal such as W, since they can have a strong effect upon the low temperature strength and brittleness. At elevated temperature, the presence of interstitial elements such as oxygen will lead to the formation of a second phases at tungsten grain boundaries and consequently lead to embrittlement [9]. Alternatively, such impurities could be removed by suitable additive to achieve a cleaner grain boundary. To restrain the formation of tungsten oxide-rich phase at elevated temperature, the direct carburization process by carbon or carbon-containing compounds can be used. The carbon balance is difficult to control and in the most cases the reduction is either incomplete or the metal powder contains carbides [10]. Nevertheless, the formation of carbides in W-matrix can have positive influence on properties of such composite for the fusion application. For instance, the use of dispersed carbides (TaC and TiC) that are distributed at the grain boundary or in the grain itself can restrict tungsten matrix grain-growth and dislocation motion, both of which lead to improved high-temperature strength and creep resistance [11, 12]. More recently, it was found that tungsten carbide (WC) additive plays a crucial role in the densification of W composites [13]. Based on these assumptions, the aim of our study is to explore and clarify the role of WC while removing oxide impurities from W matrix.

2. Materials and methods

To assess the ability of WC for oxygen binding during composite synthesis, tungsten and tungsten carbide powders in different ratios were homogenized and heated, with simultaneous application of uni-axial pressure. WC powder was mixed with tungsten powder with various C content (W−0.05 wt.% C, W−0.25 wt.% C, and W−0.51 wt.% C), calculated by stoichiometry (Table 1) based on our

estimations of free oxygen in the starting powders. The starting materials were commercially available pure W powder (99.9 % purity and particle size $\leq$ 1.5 μm, Global Tungsten & Powder) and submicron particles of WC (99 % purity and particle size in the range of 0.15 – 0.2 μm, Sigma-Aldrich). Impurities content of both used powders are listed in the supplementary date. The mixtures of WC and W powders were homogenised in cyclohexane by ultrasonic processor (UP400S, Hielscher Ultrasonic) operating at 24 kHz for 3 min at 50% amplitude. To preserve the obtained homogeneity after mixing, the suspension was freeze-dried using liquid nitrogen. Prior sintering the liquid nitrogen was removed from the mixture by sublimation under reduced pressure.

For consolidation of the powders field-assisted sintering technology device (FAST, model Dr SINTER SPS SYNTEX 3000, Fuji Electronic Industrial) was used. The powder mixtures were loaded in a graphite die with inner diameter of 16 mm.   Graphite foil was used to prevent die wear from chemical reaction with the tungsten-based powder. Prior to sintering the FAST chamber was purged with N_2 (99.996 % pure) and then evacuated (0.3 mbar - 0.5 mbar). The sintering process was carried out at vacuum conditions. The samples were heated to 1900 °C at a heating rate of 100 °C/min and a holding time of 5 min and uniaxial pressure of 60 MPa.

The crystal phase of the products after FAST consolidation were identified by X-ray diffraction (XRD, AXS D4 Endeavor, Bruker AXS), using CuKα radiation at room temperature with the diffraction angle of $2\theta = 20°$ - 80° with a step of 0.02° and acquisition time of 1.0 s/step. As already reported in our previous experiments, a reaction of the sample with graphite liner formed during sintering was observed on the surface of the sintered products [7]. To remove these artefacts, the surface reaction layer was grinded off before any further analyses.

As a consequence of the expected binary-phase composition of the product, bimodal size distribution of the grains and due to well-known challenges of the W_2C phase determination using X-ray diffraction [14-16], electron crystallography for precise phase determination was additionally employed. Electron diffraction was performed in 200 kV accelerating voltage transmission electron microscope (TEM, Jeol JEM-2100). The crystal structure of the phases was calculated from selected area electron diffraction patterns (SAEDP), and these data were used in the subsequent analyses and microstructure optimization. Samples for TEM analyses were prepared via combined mechanical (Disc grinder Mod. 623 and Dimple Grinder Mod. 656, Gatan) and Ar ion-thinning process (PIPS 691, Gatan).

The morphology of the fractured samples was studied by scanning electron microscope (SEM, JSM-7600F, Jeol) using a, operating at 15 kV. For observation of the samples' surface we used an Everhart-Thornley type detector for low-energy (<50 eV) secondary electrons (SE), generated by inelastic

scattering interactions with primary electrons. Due to their low energy, SE originates only from a few nm depth below the sample surface.

The chemical composition of the secondary phases was studied by SEM (Zeiss Auriga Crossbeam, Carl Zeiss Microscopy), employing energy-dispersive X-ray spectroscopy (EDXS; Octane Elect, EDAX AMETEK). The phase composition and their spatial distribution were assessed by electron-backscatter diffraction (EBSD; TEAM EBSD, Hikari Super, OIM Analysis software, EDAX AMETEK). Both types of experiments were conducted at an accelerating voltage of 20 kV. During image post-processing data with Confidence Index lower than 0.1 were omitted. Samples were prepared according to the standard metallographic procedures by cutting, grinding and polishing. For EBSD analyses, samples were sequentially polished with 1 μm diamond paste, and for the final polishing 5 vol. % H_2O_2 solution of colloidal silica was applied.

The oxidation resistance of the tungsten-based composites were studied by differential thermal analyses (DTA) and thermo-gravimetric analyses (TGA) (Netzsch Jupiter 449 simultaneous thermal analysis instrument coupled with Netzsch QMS 403C Aëolos quadrupole mass spectrometer (MS)). Prior to the analysis, the chamber was thoroughly purged with high purity argon (99.999 at. %) and finally evacuated (0.01 mbar). The analysis was performed using an Al_2O_3 crucible with a lid under a protective Ar atmosphere, in a temperature range of 25 °C to 1400 °C. The temperature was ramped at heating and cooling rates of 25 °C/min.

3. Results and discussion

XRD diffractograms of initial powders correspond to pure W with body-centered cubic (bcc) structure (a = 3.165 Å, Im-3m, SG: 229) and pure WC with hexagonal structure (a = b = 2.906 Å, c = 2.837 Å, P-6m2, SG: 187).
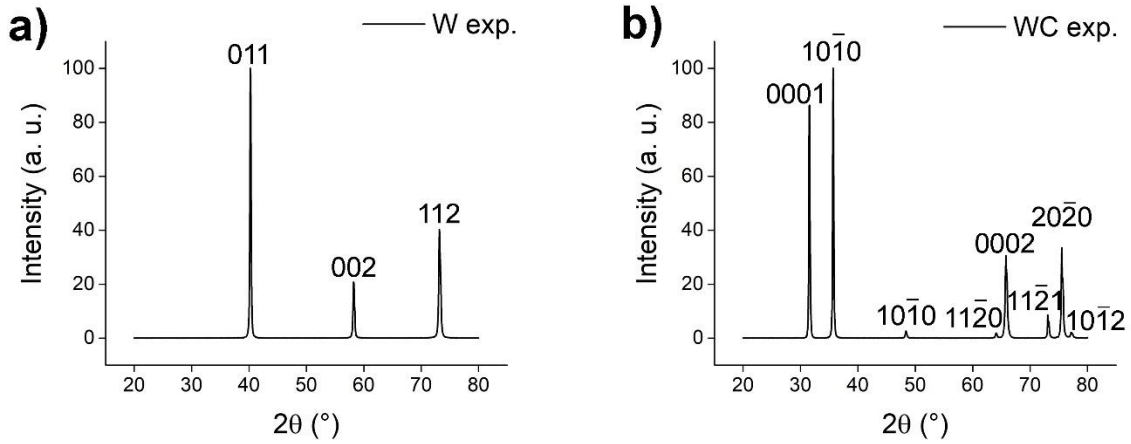
Figure 1: Experimental X-ray diffractograms of the (a) starting W (W exp.) and (b) WC powders (WC exp.). The diffracted planes of the W (ICSD #167904) [17] and WC (ICSD #5212) [18] are shown above the corresponding peaks.

For consolidated samples with compositions W−0.05WC, W−0.25WC and W−0.051WC we foresee overall carbon content of 0.7 at. %, 3.7 at. %, and 7.3 at. %, respectively (Table 1). From the W-C phase diagram [19] samples with such carbon contents would be within the W+WC two phase region at room temperature and in the W+W$_2$C two phase region after sintering at temperature higher than 1250 °C following the reaction [13]:
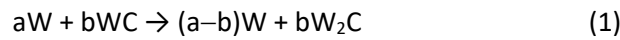
$$aW + bWC \rightarrow (a-b)W + bW_2C \qquad (1)$$

Table 1: Stoichiometry of prepared W-WC powder mixtures, expected carbon content, and calculated expected composition after FAST consolidation.

	Sample "name"		
	W−0.05WC	W−0.25WC	W−0.51WC
Carbon content (wt. %) in the starting mixture	0.05	0.25	0.51
Carbon content (at. %) in the starting mixture	0.70	3.70	7.30
Volume fraction of WC in the mixture (vol. %)	W-1.1 vol. % WC	W-4.9 vol. % WC	W-9.9 vol. % WC
Volume fraction of W$_2$C in the composite after sintering (vol. %)	W-1.9 vol. % W$_2$C	W-8.4 vol. % W$_2$C	W-17.7 vol. % W$_2$C

After the FAST consolidation, the phases formed in the bulk samples were identified. X-ray diffraction results of the consolidated bulk samples (Fig. 2a) reveal strong reflections of the bcc W. Surprisingly,

5

in the sintered samples W−0.05WC and W−0.25WC only bcc W was detected. This implies that the amount of second phase is below the detection limit of the laboratory XRD instrument (approx. 2 % [16]). In the sintered samples with the highest C content (W−0.51WC), both phases, W and W_2C (ICSD #167900 [20]), can be detected.
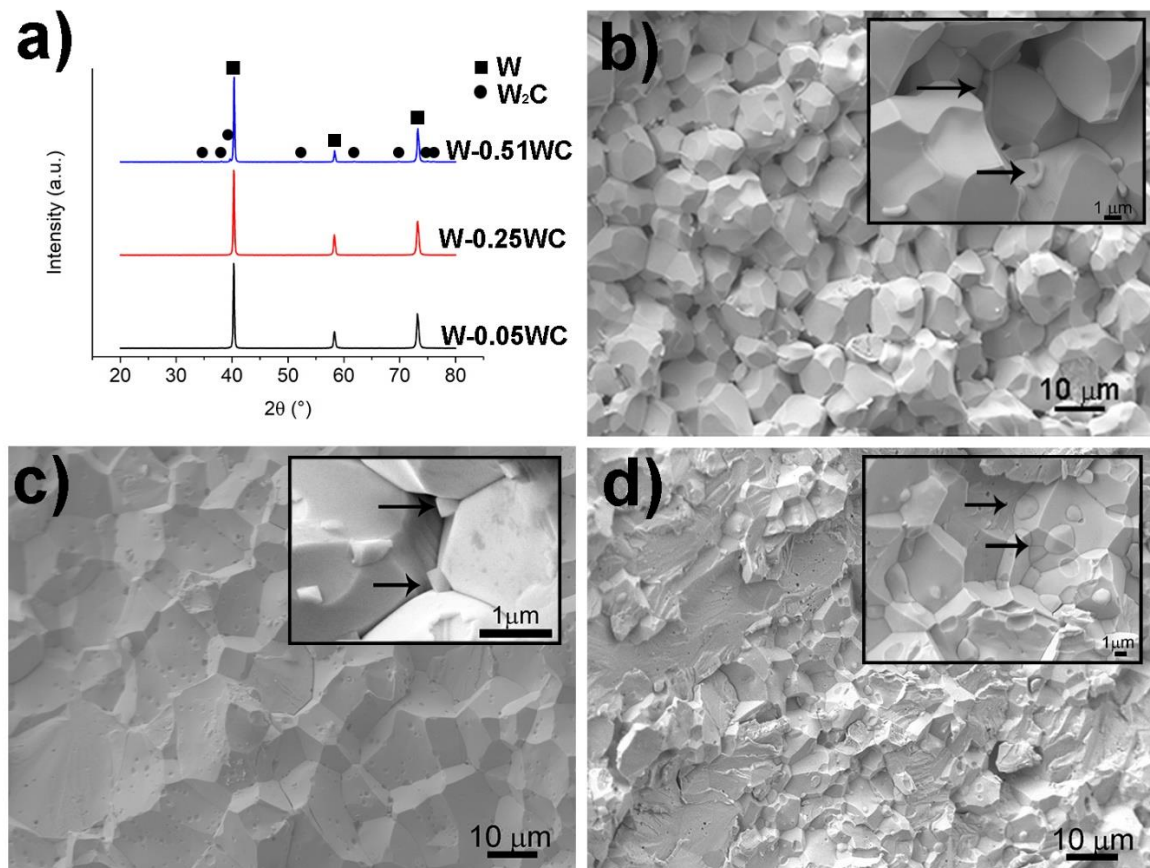

Figure 2: a) XRD patterns of W composites with different contents of WC. FE-SEM images of the fractured surface of, b) W−0.05WC, c) W−0.25W and d) W−0.51W sample. W-matrix with a secondary phase is marked with arrows.

Investigation of the morphology of the fracture surface of the sintered samples revealed different fracture modes: inter-granular and trans-granular fracture was observed on the fractured surface (Fig. 2c and Fig. 2d), while only inter-granular fracture was formed in sample W−0.05WC (Fig. 2b). The close-up inspection of the fractured composites revealed W-matrix grains, and a secondary phase located at the W grain boundaries (Inset in Fig. 2b and 2c), as well as inside W grains (Inset in Fig. 2d). By semi-quantitative EDXS mapping (Fig. 3), this secondary phase in the W−0.05WC and W−0.25WC was identified as an oxygen-rich W compound.
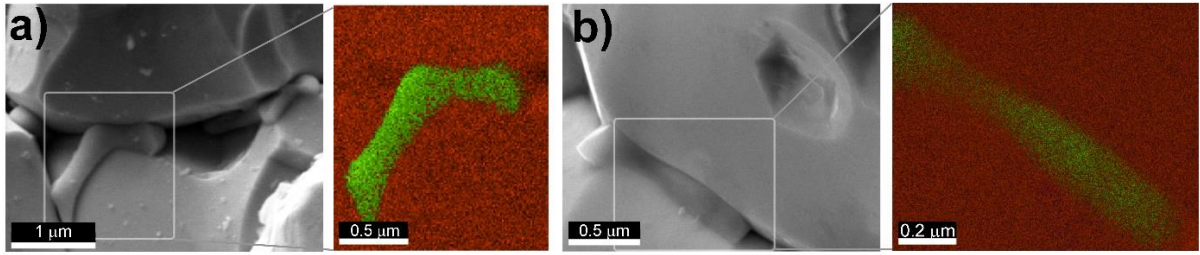
Figure 3: Secondary oxide phase adjoining W grains (SEM, SE), with the corresponding EDXS mapping for O and W (a) W–0.05WC sample and (b) W–0.25WC sample.

In the sample W−0.51WC, where W_2C was detected (Fig. 2a), the morphology and crystal structure of this secondary phase was further investigated by TEM. TEM was performed on particles located within the grains and on those at the grain bounders. Bright-field (BF) TEM images of W−0.51WC composite are presented in Figure 4. Large W grains containing single-crystal spherical grains approximately 200 nm in diameter (Fig. 4a and b), are resolved and identified by SAEDP as W_2C (insert in Fig. 4a and b). The SEADP along the [0001] and [01-10] zone axes, with the further illustrated atomic structure models in [0001] and [01-10] (Fig. 4c), from the intra-granular W_2C grains, were further indexed as a primitive trigonal/rhombohedral crystal system (lattice parameter: a, b =5.1 ± 0.5 Å and c= 4.7 ± 0.5 Å; SG: P-31m [20]), also known as ε-W_2C with the ε-Fe_2N structure.
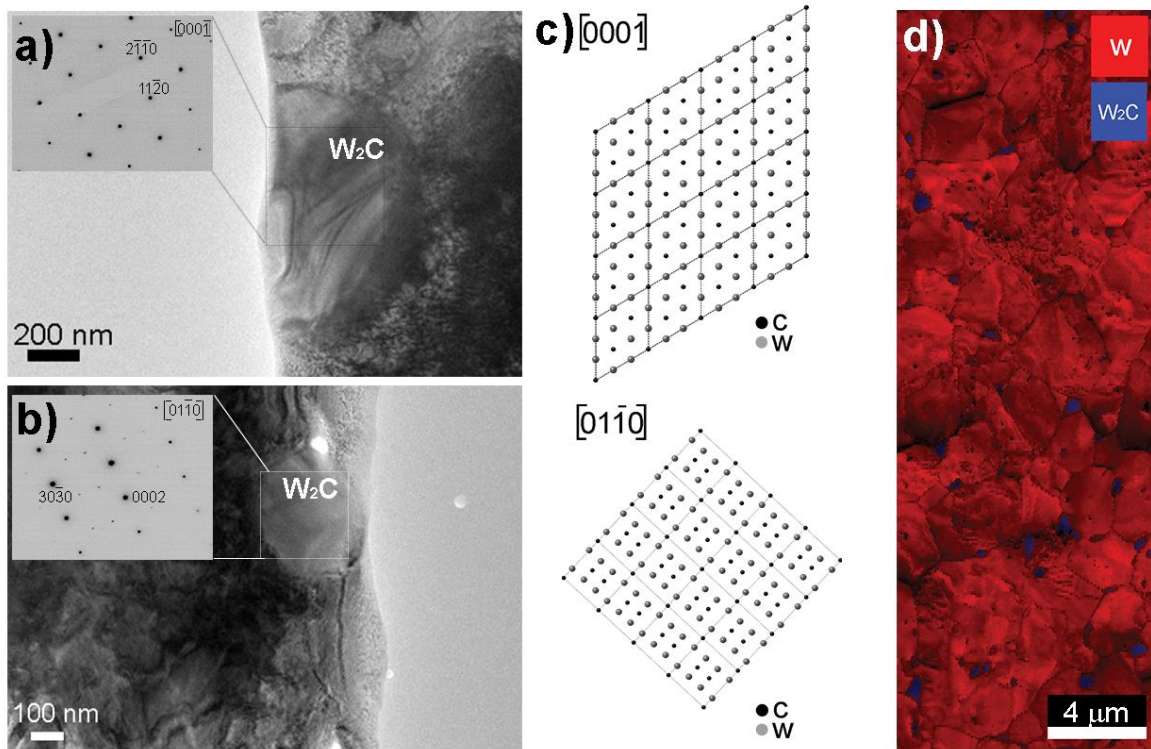

Figure 4: A TEM-BF micrographs of the W sample, containing W_2C grains embedded in W grains (a, b); inset show: (a) [0001] and (b) [01-10] zone axis SAEDP of W_2C, with the corresponding structure model in the same orientation (c). d) SEM-EBSD phase map composition with IQ maps of W (red) and W_2C (blue), constructed from crystallographic data, obtained by TEM-SAEDP. The spatial distribution

7

confirms that the larger W_2C grains are located at the W grain boundary, while numerous intra-granular W_2C crystallites are included in the W matrix.

In accordance with crystal structure determination, W_2C database were prepared for electron backscatter diffraction (EBSD) analyses, allowing to resolve this phase on larger scale. Since the differentiation of the phases is based on two different crystallographic structures, namely: cubic W and trigonal W_2C, the resulting phase map represents the spatial distribution of the W_2C phase in the W grains and at W grain boundaries (Fig. 4c). ε-W_2C does not undergo solid-phase decomposition at 1250°C and is stable at room temperature, which was also observed after different sintering process [13, 19, 21].

In accordance with the data obtain from different phase and chemical analysis, can be clearly note the deficit of W_2C phase in the tungsten-based composites studied in this research. The presence of oxygen-rich W compound after sintering suggests that oxidation occurs during consolidation with FAST. A previous study on the surface oxidation behaviour of W demonstrated that a WO_2 oxide layer grows on the tungsten surface when annealed between 727-1327 °C even in an environment with low oxygen pressure of 8×10^{-6} mbar, indicating that tungsten has a relatively poor oxidation resistance at elevated temperatures [22]. Furthermore, we reported previously that oxygen impurities in the feedstock powder could also contribute to formation of WO_2 [7]. This is attributed to the non-equilibrium conditions during the short sintering time in FAST [8]. The thermodynamically preferred reaction that can occur during FAST consolidation of the W and WC powders is the formation of WO_2:

$$W + O_2 = WO_2 \qquad (2)$$
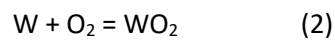
The calculation of standard Gibbs free energy ($\Delta G°$) for WO_2 formation from thermodynamic data ($\Delta H°$, $\Delta S°$) gave the following relationship: $\Delta G°=-589.7+0.1873T$ KJmol^{-1}. Based on the negative $\Delta G°$ this reaction is thermodynamically feasible and the experiments confirmed that it is also kinetically possible [7].

When surplus of C-rich additive was added (W−0.51WC), the oxygen-rich W phase disappear, which can be attributed to the reduction effect of WC. The use of graphite dies additionally ensures a reducing environment in the FAST chamber during the sintering process. To clarify these phenomena, thermo-analytical techniques were employed to determine thermal effects, evolved gasses and quantify the mass loss during heating in powder mixture W−0.51WC, for which no oxide phase was observed. Moreover, the possible reactions were considered in terms of thermodynamics.
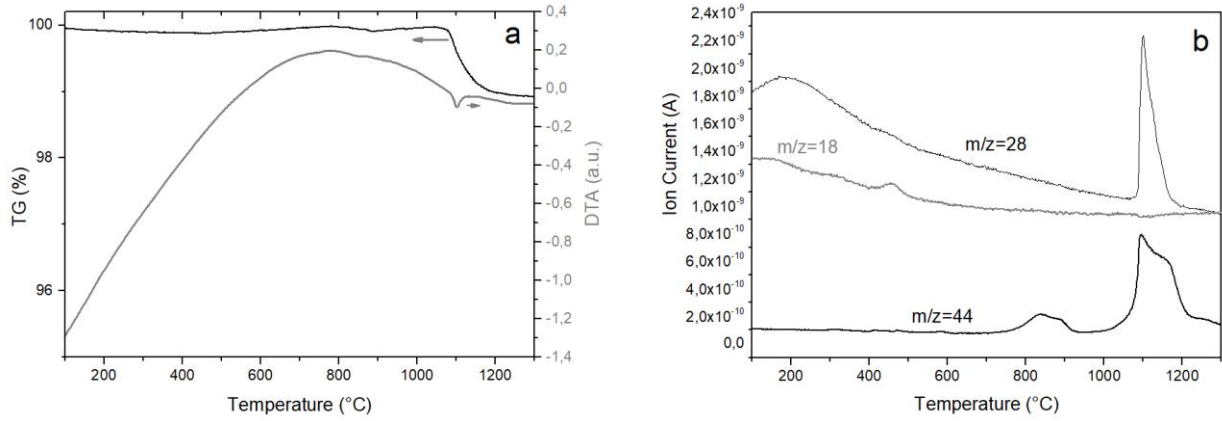
Figure 5: Thermo-gravimetric (TGA) and differential thermal analysis (DTA) curves (a) and MS of evolved gasses (b) for W−0.51WC powder composition.

For the powder mixture W−0.51WC the thermo-gravimetric (TGA) curve (Fig. 5a) demonstrate several regions of weight changes: As confirmed by mass spectrometry (MS) the first region from 25 – 350 °C with the mass loss of 0.06 % corresponds to removal of adsorbed water molecules from the surface of the powder mixture (Fig. 5b). In the temperature range from 350-780 ° C, we observed the weight gain of 0.1 %, which is associated with surface oxidation. The subsequent two steps with the total mass loss of 1.08 % was observed from 800 −1250 °C. MS revealed that both CO (m/z=28) and CO_2 (m/z=44) evolved in this temperature range. It is known that the fragment peak at m/z=28 could belong to CO_2 and to CO. Based on the difference in the peak shape and the higher intensity of the peak for m/z=28 than for m/z=44, the major contribution to the intensity of the m/z=28 peak came from CO and not from CO_2. Namely, for CO_2 the fragment m/z=28 exhibits lower intensity than the fragment m/z=44.

In the mixture of W-xWC, WC as a source of carbon will act as a reducing agent during sintering [23]. Tungsten oxide (metal oxide; MeO_2) is expected to be removed chemically by its reaction with WC, similar as it was already reported for the reaction of WC with other MeO_2 (Me-metal); $3WC+ MeO_2 \rightarrow MeC+3W+2CO$ [24].

For the reaction WC with WO_2 the following 2 reactions are proposed:

$$2WC + WO_2 \rightarrow 3W + 2CO \qquad (3)$$

$$WC + WO_2 \rightarrow 2W + CO_2 \qquad (4)$$
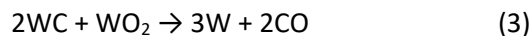
Thermodynamic consideration of both reactions revealed $\Delta G°=449.7-0.378T$ kJ mol^{-1} and $\Delta G°=236.7-0.1971T$ kJ mol^{-1}, for the reaction 3 and 4, respectively. The reaction 3, in which CO evolves, becomes thermodynamically feasible at T $\geq$ 916 °C, while the evolution of CO_2 through reaction 4 is possible at

9

T $\geq$ 928°C. The slightly more negative $\Delta G°$ of reaction 3 ($\Delta G°$ =-70 kJ mol^{-1}) compared to that of reaction 4 ($\Delta G°$ = -33 kJ mol^{-1}) at 1100 °C, where the reaction rate of the both processes reached the maximum, implied that the reaction 3 prevailed over the reaction 4. This is qualitatively supported also by the higher intensity of the peak for m/z=28 than for m/z=44. The endothermic process suggested by the above thermodynamic equations for both reactions was confirmed by the endothermic peak in the DTA curve. Formation of CO_2 is possible by combustion of C (graphite dies) or WC.

$$C + O_2 \rightarrow CO_2 \qquad (5)$$

$$1/2WC + O_2 \rightarrow 1/2WO_2 + 1/2CO_2 \qquad (6)$$
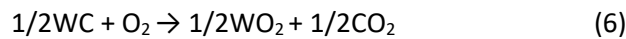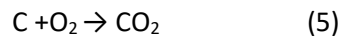
Thermodynamic analysis showed $\Delta G°$=-393.7-0.00306 T kJ mol^{-1} and $\Delta G°$=-472.35-0.089 T kJ mol^{-1} for the reactions 5 and 6, respectively. Both reactions are exothermic, what is not in accordance with the DTA results (Fig. 5a), implying that these two reactions were not dominant, although they are thermodynamically feasible ($\Delta G°<0$).

By merging the proposed reactions with the data obtained with mass spectrometry of the sample W$-$0.51WC, at least 5.8 vol. % WC (reaction 3) $-$ 8.8 vol. % WC (reaction 4) must be introduced into the starting mixture to completely remove the oxygen impurities in form of CO_2 and to obtain pure W.

During FAST consolidation of W powder at elevated temperature, the *in-situ* formation of an oxide-rich tungsten phase was observed also reported by other researchers [7-9]. The degradation of W-based composites containing an oxide-rich tungsten phase at elevated temperature will influence the performance of such material when used as plasma facing material for fusion application [7]. For the future designing of plasma facing material, we need to mitigate the influence of small amounts of oxygen or completely remove it by carburization reaction. During an accident in a fusion reactor, such as a failure of the cooling system, the nuclear decay heat can cause the first wall to heat up significantly (up to 1127 °C). If air enters the fusion reactor chamber, tungsten will start to form highly volatile tungsten oxide compounds that in worst case even escape the chamber [3]. Development of self-passivating W-based composted can improve the intrinsic safety of future fusion facilities. A previous study suggest that W_2C as a source of carbon can also remove other metal oxide species via reaction [24]:

$$W_2C + MeO_2 \rightarrow MeC + 6W + 2CO \text{ or: } W_2C + WO_2 \rightarrow WC + 2W + 2CO \qquad (7)$$
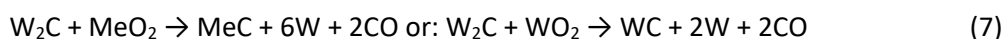
Based on the $\Delta G°$=358.14-0.439T kJ mol^{-1} the reaction W_2C + WO_2 $\rightarrow$ WC + 2W + 2CO is thermodynamically feasible at T $\geq$ 542 °C.

To evaluate the suitability of W/W_2C composite as plasma facing material, the microstructure of the composite still needs to be characterized after neutron and ion bombardment and after high heat-load experiments.

4. Conclusion

In-situ formation of an oxide-rich tungsten phase in the W matrix during high-temperature vacuum consolidation in FAST must be taken into account when considering fusion application. In this work, trace amounts of oxide impurities were identified and removed by the use of carbon in form of WC deoxidation agent. Based on the calculation at least 5.8 vol. % WC $-$ 8.8 vol. % WC must be introduced into the starting mixture to completely remove the oxygen impurities in form of CO_2 and to obtain pure W. However, the surplus amount of WC will lead to the formation of a second phase, W_2C at 1900 °C.

Acknowledgements

References

1.   D. Maisonnier, D. Campbell, I. Cook, L. Di Pace, L. Giancarli, J. Hayward, A. Li Puma, M. Medrano, P. Norajitra, P. Sardain, M. Q. Tran, and D. Ward *Power plant conceptual studies in Europe.* Nucl. Fusion, 2007. **47**(11): p. 1524-1532.
2.   G. Pintsuk, *Tungsten as a Plasma-Facing Material.* Comprehensive Nuclear Materials, R. J. M. Konings (Ed.). Vol. 4. 2012, Amsterdam: Elsevier. 551-581. https://doi.org/10.1016/B978-0-08-056033-5.00118-X.
3.   J. W. Coenen, S. Antusch, M. Aumann, W. Biel, J. Du, J. Engels, S. Heuer, A. Houben, T. Hoeschen, B. Jasper, and F. Koch, J. Linke, A. Litnovsky, Y. Mao, R. Neu, G. Pintsuk, J. Riesch, M. Rasinski, J. Reiser, M. Rieth, A. Terra, B. Unterberg, Th. Weber, T. Wegener, J-H You and Ch. Linsmeier, *Materials for DEMO and reactor applications—boundary conditions and new concepts.* Phys. Scr., 2016. **2016**: p. 014002. https://doi.org/10.1088/0031-8949/2016/T167/014002

4.   Z. Z. Fang, *Sintering of Advanced Materials - Fundamentals and processes*. 2010, Cambridge, UK: Woodhead Publishing.
5.   J. Choi, H.-M. Sung, K.-B. Roh, S.-H. Hong, G.-H. Kum, and H.-N. Han, *Fabrication of sintered tungsten by spark plasma sintering and investigation of thermal stability.* Int. J. Refract. Met. H, 2017. **69**: p. 164-169. https://doi.org/10.1016/j.ijrmhm.2017.08.013.

6.   G. Lee, J. McKitrick, E. Ivanov, and E. A. Olevsky, *Densification mechanism and mechanical properties of tungsten powder consolidated by spark plasma sintering.* Int. J. Refract. Met. H., 2016. **61**: p. 22-29. http://dx.doi.org/10.1016/j.ijrmhm

7.   A. Šestan, P. Jenuš, S. K. Novak, J. Zavašnik, and M. Čeh, *The role of tungsten phases formation during tungsten metal powder consolidation by FAST: Implications for high-temperature applications.* Mater. Charact., 2018. http://dx.doi.org/10.1016/j.matchar.2018.02.022

8.   L. Huang, L. Jiang, T. D. Topping, C. Dai, X. Wang, R. Carpenter, C. Haines, and J. M. Schoenung, *In situ oxide dispersion strengthened tungsten alloys with high compressive strength and high strain-to-failure,.* Acta Mater., 2017. **122**: p. 19-31. https://doi.org/10.1016/j.actamat.2016.09.034

9.   J. R. Stephens, *Effects of Interstitial Impurities on the Low-Temperature Tensile Properties of Tungsten*, in *NASA Technical Note D-2287*. 1964: Washington, D. C.

10.   E. Lassner and W.-D. Schubert, *Tungsten: Properties, Chemistry, Technology of the Element, Alloys, and Chemical Compounds*. 1999 New York: Springer US.

11.   X.-Y. Tan , L.-M. Luo, Z.-L. Lu, G.-N. Luo, X. Zan, J.-G. Cheng, and Y.-C. Wu, *Development of tungsten as plasma-facing materials by doping tantalum carbide nanoparticles.* Powder Technol., 2015. **269**: p. 437-442. https://doi.org/10.1016/j.powtec.2014.09.039

12.   G. M. Song, , Y. Zhou, and Y.J. Wang, *The microstructure and elevated temperature strength of tungsten-titanium carbide composite.* J. Mater. Sci. 2002. **37**(16): p. 3541-3548. https://doi.org/10.1023/A:1016583611632

13.   S. Chanthapan, A. Kuklkarni, J. Singh, C. Hains, and D. Kapoor, *Sintering of tungsten powder with and without tungsten carbide additive by field assisted sintering technology.* Int. J. Refract. Met. H., 2012. **31**: p. 114-120. https://doi.org/10.1016/j.ijrmhm.2011.09.014

14.   T. Epicier, J. Dubois, C. Esnouf, G. Fantozzi, and P. Convert , *Neutron powder diffraction studies of transition metal hemicarbides M2C1−x—II. In situ high temperature study on W2C1−x and Mo2C1−x.* Acta Metall., 1988. **36**(8): p. 1903-1921. https://doi.org/10.1016/0001-6160(88)90293-3

15.   A. S. Kurlov and A.I. Gusev, *Neutron and x-ray diffraction study and symmetry analysis of phase transformations in lower tungsten carbide W_2C.* Phys. Rev. B, 2007. **76**(17): p. 174115. https://doi.org/10.1103/PhysRevB.76.174115

16.   D. L. Bish and J.E. Post, *Modern powder diffraction*. 1989: Mineralogical Society of America.

17.   A. Friedrich, B. Winkler, L. Bayarjargal, A. Juarez, A. Erick, W. Morgenroth, J. Biehler, F. Schroeder, J. Yan, and S. M. Clark, *In situ observation of the reaction of tantalum with nitrogen in a laser-heated diamond anvil cell.* J. Alloys and Compd, 2010. **42**(no. 17). https://doi.org/10.1016/j.jallcom.2010.04.113

18.   Q. Fang , W. Bai, J. Yang , X. Xu, G. Li , Shi N. ,M. Xiong, and H. Rong *Qusongite (WC): A new mineral.* Am. Mineral., 2009. **94**: p. 387-390. https://doi.org/10.2138/am.2009.3015

19.   A. S. Gusev and A. I. Gusev, *Tungsten Carbides: Structure, Properties and Application in Hardmetals*. Springer Series in Materials Science, C. J. R. Hull, R. M. Osgood, J. Parisi, Z. M. Wang (Eds.), Vol. 184. 2013: Springer International Publishing.

20.   Y.-F. Li, Y.-M. Gao, B. Xiao, T. Min, Z.-J. Fan, S.-Q. Ma, and L.-L. Xu, *Theoretical study on the stability, elasticity, hardness and electronic structures of W-C binary compounds.* J. Alloys Compd, 2010. **502**: p. 28-37. https://doi.org/10.1016/j.jallcom.2010.04.184

21.   T. Li, Q. Li, J. Y. H. Fuh, P. C. Yu, and C. C. Wu, *Effects of lower cobalt binder concentrations in sintering of tungsten carbide.* Mater. Sci. Eng. A, 2006. **430**(1): p. 113-119. https://doi.org/10.1016/j.msea.2006.05.118

22.   K. Radican, I. S. Bozhko, S. - R. Vadapoo, S. Ulucan, H.-C. Wu, A. McCoy, and I.V. Shvets, *Oxidation of W(110) studied by LEED and STM.* Surf. Sci., 2010. **604**(19): p. 1548-1551. https://doi.org/10.1016/j.susc.2010.05.016

23. J. Zou, H.- B. Ma, A. D'Angio, and G.- J. Zang , *Tungsten carbide: A versatile additive to get trace alkaline-earth oxide impurities out of ZrB2 based ceramics.* Scripta Mater., 2018. **147**: p. 40-44. https://doi.org/10.1016/j.scriptamat.2017.12.033

24. G.-J. Zhang, H.-T. Liu, W.-W. Wu, J. Zou, D.-W. Ni, W.-M. Guo, J.-X. Liu, and X.-G. Wang, Reactive Processes for Diboride-Based Ultra-High Temperature Ceramics, in: W.G. Fahrenholtz, E. J. Wuchina, W. E. Lee, and Y. Zhou (Eds.), *Ultra-High Temperature Ceramics: Materials for Extreme Environment Applications*, 2014: Wiley.